Nuclear Engineering and Technology 51 (2019) 2018–2025

Contents lists available at ScienceDirect

Nuclear Engineering and Technology

journal homepage: www.elsevier.com/locate/net

Original Article

Comparing the performance of two hybrid deterministic/Monte Carlo transport codes in shielding calculations of a spent fuel storage cask

Po-Chen Lai [a], Yu-Shiang Huang [a, b], Rong-Jiun Sheu [a, c, *]

[a] Institute of Nuclear Engineering and Science, National Tsing Hua University, Hsinchu, 30013, Taiwan, ROC
[b] Nuclear Science and Technology Development Center, National Tsing Hua University, Hsinchu, 30013, Taiwan, ROC
[c] Department of Engineering and System Science, National Tsing Hua University, Hsinchu, 30013, Taiwan, ROC

ARTICLE INFO

Article history:
Received 29 June 2018
Received in revised form
13 June 2019
Accepted 19 June 2019
Available online 20 June 2019

Keywords:
hybrid deterministic/Monte Carlo transport code
CADIS methodology
Spent nuclear fuel
Storage cask
Dose rate distribution

ABSTRACT

This study systematically compared two hybrid deterministic/Monte Carlo transport codes, ADVANTG/MCNP and MAVRIC, in solving a difficult shielding problem for a real-world spent fuel storage cask. Both hybrid codes were developed based on the consistent adjoint driven importance sampling (CADIS) methodology but with different implementations. The dose rate distributions on the cask surface were of primary interest and their predicted results were compared with each other and with a straightforward MCNP calculation as a baseline case. Forward-Weighted CADIS was applied for optimization toward uniform statistical uncertainties for all tallies on the cask surface. Both ADVANTG/MCNP and MAVRIC achieved substantial improvements in overall computational efficiencies, especially for gamma-ray transport. Compared with the continuous-energy ADVANTG/MCNP calculations, the coarse-group MAVRIC calculations underestimated the neutron dose rates on the cask's side surface by an approximate factor of two and slightly overestimated the dose rates on the cask's top and side surfaces for fuel gamma and hardware gamma sources because of the impact of multigroup approximation. The fine-group MAVRIC calculations improved to a certain extent and the addition of continuous-energy treatment to the Monte Carlo code in the latest MAVRIC sequence greatly reduced these discrepancies. For the two continuous-energy calculations of ADVANTG/MCNP and MAVRIC, a remaining difference of approximately 30% between the neutron dose rates on the cask's side surface resulted from inconsistent use of thermal scattering treatment of hydrogen in concrete.

1. Introduction

Dry casks are the most common method of interim storage for spent nuclear fuels until a permanent repository is decided and made available. A dry storage cask typically has a steel container that provides leak-tight containment of spent fuels. Additional shielding materials such as concrete, metal, or neutron absorbers surrounded the container to reduce dose rates outside the cask. In Taiwan, radiation shielding analysis of an interim dry storage facility is not only a critical topic for applicant and regulatory bodies but also a concern for nearby residents and the public because of a relatively short distance to site boundaries and the currently overwhelming anti-nuclear atmosphere. A stringent design dose limit of 0.05 mSv per year at the nearest site boundary was promised by the state-run Taiwan Power Company (Taipower) [1], compared with a typical value of 0.25 mSv per year adopted in most countries [2] for direct radiation from an independent spent fuel storage installation (ISFSI). Therefore, simplified but conservative assessment methods were unfavorable; instead, accurate three-dimensional (3D) transport calculations were primarily used in shielding analyses to minimize the margins of conservatisms and uncertainties. For the two approved ISFSI facilities in Taiwan, a great deal of computational effort was spent in relevant analyses during the design phase and review process because many repeated calculations were necessary to optimize and verify the shielding requirements.

A high-fidelity shielding analysis of an ISFSI involves numerous computational challenges, including multiple source terms, complicated geometries of the cask and facility, neutron and gamma-ray deep-penetration calculations, radiation streaming through cooling ducts, and skyshine evaluations. The Monte Carlo

* Corresponding author. Institute of Nuclear Engineering and Science, National Tsing Hua University, Hsinchu, 30013, Taiwan, ROC.
E-mail address: rjsheu@mx.nthu.edu.tw (R.-J. Sheu).

https://doi.org/10.1016/j.net.2019.06.019

method is a suitable choice for the task and has gradually become the preferred method because of its powerful capabilities in problem modeling and calculation accuracy. However, Monte Carlo results inherently contain statistical uncertainties that decrease inversely with the square root of the number of histories being simulated. Convergence to a desired tolerance can be extremely time-consuming; this limitation hinders Monte Carlo simulations for being applied to many real-world shielding problems. To render a challenging Monte Carlo simulation computationally feasible and practical, powerful hardware and effective variance reduction techniques are indispensable.

Combining the advantages of deterministic and Monte Carlo methods in transport calculations has been an important direction in the recent development of advanced methodologies. The benefits of using deterministic adjoint functions in Monte Carlo variance reduction techniques are well known. The consistent adjoint driven importance sampling (CADIS) methodology is one of the major achievements in this trend [3,4]. In this study, the authors adopted two calculation tools, ADVANTG/MCNP [5] and MAVRIC [6], to re-examine a cask shielding problem described in the safety analysis report (SAR) of the ISFSI at the Kuosheng nuclear power plant in Taiwan [1]. Dose rate distributions on the top and side surfaces of a storage cask were of primary interest. Skyshine and dose rates at site boundary were not discussed in this study. Both ADVANTG/MCNP and MAVRIC were developed based on the CADIS methodology but with different implementations in the last-step biased Monte Carlo simulations. Their calculation results were compared with each other as well as with a straightforward MCNP [7] calculation with default settings in physics and variance reduction. The performances of these three codes were compared and evaluated in terms of their accuracies in dose rate predictions and associated computational efficiencies. ADVANTG/MCNP and MAVRIC have become increasingly popular in recent studies of fixed-source shielding analyses. For example, Thiele and Börst [8] performed shielding benchmark calculations with MAVRIC and compared with dose rate measurements for a single CASTOR cask. Wagner et al. [9] provided a review of the hybrid transport methods and codes used at the Oak Ridge National Laboratory and considered a spent fuel cask shielding problem as an illustration of their application. Regarding comparisons of the two codes, Matijević et al. [10] and Paul [11] presented comparative studies of dose rate calculations for a spent fuel pool and for the ES-3100 package with highly enriched uranium content, respectively, using different computational shielding methodologies, including ADVANTG/MCNP and MAVRIC. To the best of the authors' knowledge, most related studies have involved only one of them or have lacked systematic comparisons between the two codes when applied to a practical shielding problem. This motivated us to conduct the present study. Focusing on a real-world storage cask for spent nuclear fuels, ADVANTG/MCNP and MAVRIC were applied to solve the same problem of determining dose rate distributions on a cask's top and side surfaces. The comparison results and experience obtained should be helpful to users of these two codes and those performing similar shielding analyses.

2. Materials and methods

2.1. Spent nuclear fuel and storage cask

The Kuosheng nuclear power plant is the largest nuclear power plant in Taiwan, possessing two units of General Electric's boiling water reactor (BWR) type 6 with a total electricity output of 2×985 MW_e. The plant has been operated commercially for more than 35 years. Because its spent fuel pool is near to capacity, Taipower proposed an ISFSI facility at the plant site for interim dry storage of spent nuclear fuels. The phase one plan was approved with a capacity of 27 storage casks. According to its SAR [1], the storage cask was essentially the MAGNASTOR type developed by NAC International Inc [12] with some shielding enhancements to comply with the stringent dose limit at the site boundaries. Fig. 1 shows the geometric model of the cask used in this study, which had overall dimensions of approximately 6 m in height and 4.3 m in diameter. The model included a detailed description of the canister and shielding structure. The canister was able to accommodate 87 BWR spent fuel assemblies. Outside the canister, a steel liner, concrete shielding, air inlets/outlets, and other supporting structures were present. Shielding against radiation from spent nuclear fuels is mainly achieved using steel and concrete; in total, approximately 11.27 cm thick steel and 101.5 cm thick concrete formed the cask's side shielding and approximately 27.86 cm thick steel and 66.7 cm thick concrete formed its top shielding. For the detailed dimensions of the cask model and their material assignments, please refer to the SAR [1].

The design-basis spent fuel was a GE8 $\times$ 8-2 fuel assembly with an initial U-235 enrichment of 2.84%, maximum burnup of 34 GWD/MTU, and cooling for 20 years. Each fuel assembly was modeled in four consecutive regions; from top to bottom, these were the upper end fitting (UEF), plenum, effective fuel, and lower end fitting (LEF) regions. Three radiation sources were considered for shielding calculations: fuel neutron (FN), fuel gamma (FG), and hardware gamma (HG). FN and FG sources resulting from actinides and fission products in spent fuels were contained only in the effective fuel region. In addition, HG sources existed in all regions, mainly due to neutron activation in their structural materials. Table 1 lists the regional intensities of these three radiation sources in the canister, corresponding to a full loading of 87 design-basis spent fuels. Uniform spatial distribution was assumed for source terms in the UEF, plenum, and LEF regions. The axial distributions of source terms in the effective fuel region were derived from the burnup profile of the design-basis spent fuel. The detailed energy and spatial distributions used in shielding simulations were the same as those adopted in the SAR; they are omitted here for brevity.

2.2. Calculation tools

Two hybrid deterministic/Monte Carlo transport codes, ADVANTG/MCNP and MAVRIC, were employed to estimate the dose rate distributions on the top and side surfaces of the aforementioned storage cask, as illustrated in Fig. 1. The acronym ADVANTG/MCNP denotes the ADVANTG automated variance reduction generator (version 3.0.3) coupled with MCNP5 version 1.60. The

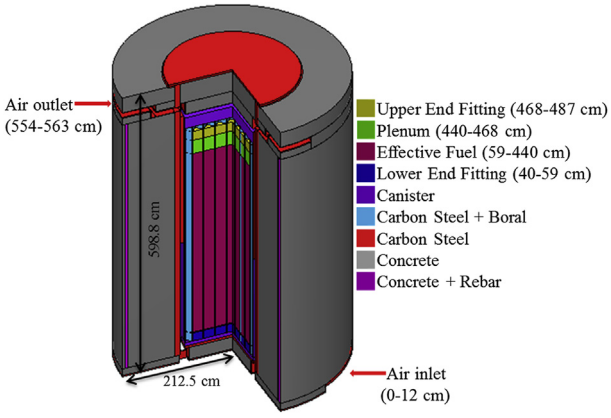

Fig. 1. Cutaway view of the cask geometry model.

Table 1
Total source intensities of 87 spent fuels in the MAGNASTOR cask.

Source	Region	Strength (n or γ/s/cask)
Fuel neutron (FN)	Effective fuel	4.799×10^{09}
Fuel gamma (FG)	Effective fuel	6.581×10^{16}
Hardware gamma (HG)	Lower end fitting (LEF)	6.020×10^{13}
	Effective fuel	2.818×10^{13}
	Plenum	3.757×10^{13}
	Upper end fitting (UEF)	1.793×10^{13}

MAVRIC sequence in the latest release of the SCALE code system, version 6.2.2, was also used to solve the same shielding problem for comparison with ADVANTG/MCNP. Both hybrid codes implement the CADIS methodology for generating variance reduction parameters for fixed-source Monte Carlo simulations. The variance reduction parameters consist of space and energy-dependent weight windows and a consistent biased source distribution, both of which take advantage of an approximate adjoint transport solution generated by the 3D multigroup discrete ordinates code Denovo [13]. The CADIS methodology was originally developed to optimize a single tally; however, the variance reduction parameters can be optimized for multiple tallies by using an extension approach called the Forward-Weighted CADIS (FW-CADIS) method [14], which requires an additional Denovo calculation in the forward mode.

Regarding the difference between ADVANTG/MCNP and MAVRIC in CADIS methodology implementation, MAVRIC passed the generated variance reduction parameters to the 3D Monte Carlo shielding code Monaco [15] in the SCALE code package, whereas ADVANTG was designed for direct use with unmodified versions of MCNP5. Prior to SCALE 6.2, one of the key differences between MAVRIC and ADVANTG/MCNP in terms of transport physics was the format of the underlying cross sections. MCNP can perform continuous-energy Monte Carlo transport calculations, whereas Monaco supports only multigroup format data libraries. Multigroup cross sections are problem-dependent, and this approximation in the cross-section representation could be problematic in some situations, such as in neutron deep-penetration calculations in iron. Implementation of continuous-energy physics in Monaco [16] extends the capabilities of MAVRIC to higher-fidelity simulations. Therefore, performing a detailed comparison study between MAVRIC and ADVANTG/MCNP in a real-world shielding problem becomes more enlightening and valuable. In addition to hybrid methods, although MCNP itself is rich in variance reduction features, a straightforward MCNP simulation without user-specified variance reduction techniques was conducted as a baseline case for measuring the performance of the two hybrid codes.

2.3. Numerical settings

For a complicated real-world shielding problem such as the present case, performing a fair comparison between various Monte Carlo transport codes that were developed with different considerations and implementations is difficult. Nevertheless, the authors endeavored to make the comparisons in this study as reliable as possible by carefully checking the calculation models built using three codes, ADVANTG/MCNP, MAVRIC, and the straightforward MCNP, to ensuring that they had identical geometry, material, source, and detector descriptions. The geometric dimensions and composition assignments between models were verified by searching and comparing not only values specified in the input files but also those echoed in the output files. In addition, particle transport in models with materials assigned to void was performed to verify the consistency of source and detector definitions in different models.

The dose rate distributions on the top and side surfaces of the storage cask were the main target of this study. To achieve more uniform statistical uncertainties in these tally regions, the FW-CADIS method was activated in the hybrid simulations to optimize the objective of uniform particle tracks on the cask's top and side surfaces. FW-CADIS implementation in MAVRIC and ADVANTG/MCNP simulations requires additional discrete ordinates calculations in the forward and adjoint modes, respectively. Because only approximate solutions were required for this purpose, the spatial discretization of the problem domain was chosen to be rather coarse to represent the large and complicated storage cask in a few of XYZ meshes ($98 \times 98 \times 58$). In the adjoint mode calculation, a thin volume source covering the entire cask surface above the ground was defined to attract particles in the subsequent Monte Carlo simulation to move as outwardly as possible. The energy spectrum of the adjoint source was defined as the flux-to-dose rate conversion factors used in dose rate calculations. The FW-CADIS method further helped to spread particles over phase space, leading to relatively uniform statistical uncertainties across mesh tallies on the cask's top and side surfaces.

For the Denovo discrete ordinates calculations, the 27N19G multigroup cross-section set in the SCALE library was used for both the forward and adjoint modes. The calculations were performed with a P3 Legendre expansion of scattering anisotropy and an S8 angular quadrature set. For Monaco Monte Carlo calculations, three data sets—including the 27N19G and 200N47G multigroup as well as CE continuous-energy cross sections in the SCALE libraries—were used individually, and their results were compared to investigate the effect of cross sections on the accuracy of surface dose rate predictions. Notably, all of these cross-section data sets in SCALE and that used in continuous-energy MCNP calculations were derived from the same version of the ENDF/B-VII.0 library.

In addition to mesh tallies covering the cask's surface, the average dose rate on the cask's top surface was scored by a thin circular disk with a radius of 92 cm, which was identical to that of the effective fuel region. Similarly, the average dose rate on the side surface was defined by scoring a cylindrical shell with a height of 382 cm that also covered the effective fuel region. The two cell tallies were arranged to indicate the average dose levels on the cask surfaces and to facilitate comparison of computational efficiencies among various calculations. Dose rates were obtained by folding the calculated neutron and gamma-ray spectra with appropriate flux-to-dose rate conversion factors. The computational efficiency was defined using the figure of merit (FOM), which is the inverse of the product of the error squared and total computing time in minutes. The higher the FOM, the greater the computational efficiency.

3. Results and discussion

Considering the three source terms (FN, FG, and HG) in this shielding problem, three separate fixed-source simulations were necessary for a complete analysis of dose rate distribution around the storage cask. This study evaluated and compared the performances of three Monte Carlo codes in five cases; as described in the previous section, these cases were MCNP, ADVANTG/MCNP, and three MAVRIC runs with different cross-section libraries, labeled as MG-27N19G, MG-200N47G, and CE. A total of 15 simulations were performed. The execution time of each simulation was purposely limited to approximately 1 day for an intuitive comparison of the resultant statistical uncertainties. All calculations were conducted on a Windows 7 computer equipped with an Intel Core i7-3770 (3.4 GHz) processor and 16 GB RAM. Table 2 lists the computing times of these simulations, including those spent in forward and

Table 2
Computation times of 15 simulations in this study involving three Monte Carlo codes in five cases (MCNP, ADVANTG/MCNP, and three MAVRIC runs with different cross-section sets) for three different source terms (FN, FG, and HG), including the computation times spent in discrete ordinates (S_N) and Monte Carlo (MC) calculations.

	Source	Forward S_N (min)	Adjoint S_N (min)	Total S_N (min)	MC (hr)	Total (hr)
MCNP	FN	n/a	n/a	n/a	26.01	26.01
	FG	n/a	n/a	n/a	26.00	26.00
	HG	n/a	n/a	n/a	26.00	26.00
ADVANTG/MCNP	FN	37.62	27.46	67.52	24.89	26.02
	FG	7.14	9.00	17.38	25.72	26.01
	HG	6.50	8.85	16.56	25.74	26.01
MAVRIC (MG-27N19G)	FN	35.87	21.03	56.90	27.00	27.94
	FG	6.67	6.38	13.05	25.90	26.09
	HG	6.68	8.11	14.79	26.00	26.23
MAVRIC (MG-200N47G)	FN	30.99	20.78	51.77	25.20	26.07
	FG	6.61	6.79	13.39	25.50	25.76
	HG	5.67	6.81	12.49	25.70	25.97
MAVRIC (CE)	FN	30.84	20.79	51.64	26.30	27.16
	FG	6.68	6.75	13.44	26.00	26.24
	HG	5.67	6.75	12.42	26.10	26.29

adjoint discrete ordinates calculations that were necessary for FW-CADIS acceleration. The discrete ordinates calculations—either in forward or adjoint modes—required between 5 and 15 min for gamma source problems; more time was required (up to 1 h) for the FN cases that involved neutron/gamma-coupled transport. The computing time for a 3D discrete ordinates calculation can be long, mainly depending on the size of phase space discretization and required accuracy of the solution. In general, instead of pursuing a precise solution, obtaining a discrete ordinates solution with approximately the correct shape is sufficient for variance reduction. Notably, this approximate solution did not compromise the intrinsic accuracy of the subsequent Monte Carlo simulation based on detailed 3D geometry, continuous energy and angular treatments.

3.1. Accuracies of predicted dose rates

Table 3 compares the average surface dose rates on the cask's top and side surfaces calculated by MCNP, ADVANTG/MCNP, and three MAVRIC simulations. For the FN source case, the straightforward MCNP calculation obtained reasonable estimates in an affordable computing time. As expected, the results of the hybrid ADVANTG/MCNP calculation were consistent with the MCNP, and more importantly, the variance reduction scheme resulted in overall improvements in computational efficiency, especially for two neutron tallies that yielded improvements of approximately two orders of magnitude. The speedup was measured as the FOM ratio between two runs. Also based on the FW-CADIS methodology, MAVRIC in this case generally achieved similar or slightly lower performance in computational efficiency when compared with ADVANTG/MCNP. However, the 27N19G multigroup MAVRIC calculation tended to underestimate the neutron and induced gamma dose rates on the cask's side surface and overestimate the corresponding dose rates on the cask's top surface to varying degrees when compared with the MCNP or ADVANTG/MCNP results. The MCNP-related calculations with continuous-energy cross-section data were generally considered more accurate and reliable than those obtained using multigroup calculations, especially for deep-penetration calculations. The 200N47G fine-group and continuous-energy MAVRIC calculations generally mitigated these discrepancies but still underestimated the neutron dose rate on the cask's side surface by approximately 30% and underestimated the induced gamma dose rates on the cask's surfaces by 10–15%, when the ADVANTG/MCNP prediction was used as a reference.

The FG source consisted mostly of low-energy gamma rays. The straightforward MCNP calculation in this case recorded nothing on

Table 3
Comparisons of average dose rates on the cask's top and side surfaces calculated by MCNP, two ADVANTG/MCNP runs, and three MAVRIC runs with different cross-section sets.

Src.		MCNP			ADVANTG/MCNP			MAVRIC (MG27n19g)		
	Det.	Dose rate (mSv/h)	Error (%)	FOM	Dose rate (mSv/h)	Error (%)	FOM	Dose rate (mSv/h)	Error (%)	FOM
FN	Side n	3.14×10^{-5}	7.37	0.12	3.49×10^{-5}	0.58	19	1.78×10^{-5}	0.68	13
	Top n	1.46×10^{-4}	18.03	0.02	1.84×10^{-4}	2.42	1.09	2.53×10^{-4}	3.51	0.50
	Side γ	3.19×10^{-4}	0.57	20	3.18×10^{-4}	0.70	13	2.77×10^{-4}	1.05	5.60
	Top γ	1.90×10^{-4}	3.80	0.44	1.91×10^{-4}	1.66	2.32	2.26×10^{-4}	3.88	0.41
FG	Side γ	-	-	-	4.99×10^{-5}	0.09	791	7.21×10^{-5}	0.11	564
	Top γ	-	-	-	2.12×10^{-4}	8.12	0.10	2.74×10^{-4}	3.99	0.41
HG	Side γ	3.48×10^{-6}	78.23	0.001	8.78×10^{-6}	0.11	530	1.56×10^{-5}	0.12	475
	Top γ	2.63×10^{-4}	43.45	0.003	3.56×10^{-4}	1.12	5.11	4.84×10^{-4}	2.01	1.59
		MAVRIC (MG200n47g)			MAVRIC (CE)			ADVANTG/MCNP (Sab)		
Src.	Det.	Dose rate (mSv/h)	Error (%)	FOM	Dose rate (mSv/h)	Error (%)	FOM	Dose rate (mSv/h)	Error (%)	FOM
FN	Side n	2.38×10^{-5}	0.65	16	2.47×10^{-5}	1.01	6.19	2.52×10^{-5}	0.70	13
	Top n	1.44×10^{-4}	5.30	0.24	1.89×10^{-4}	5.00	0.25	1.76×10^{-4}	2.35	1.16
	Side γ	2.63×10^{-4}	0.93	7.66	2.62×10^{-4}	1.36	3.41	2.68×10^{-4}	0.90	7.91
	Top γ	1.72×10^{-4}	3.29	0.61	1.73×10^{-4}	3.54	0.51	1.63×10^{-4}	1.57	2.60
FG	Side γ	5.04×10^{-5}	0.12	454	4.95×10^{-5}	0.14	345	5.00×10^{-5}	0.09	791
	Top γ	2.34×10^{-4}	4.46	0.33	2.24×10^{-4}	6.90	0.14	2.12×10^{-4}	7.94	0.10
HG	Side γ	8.98×10^{-6}	0.13	372	8.77×10^{-6}	0.15	286	8.78×10^{-6}	0.11	530
	Top γ	3.76×10^{-4}	2.63	0.93	3.65×10^{-4}	2.41	1.11	3.56×10^{-4}	1.11	5.20

the cask's surfaces during the 26-h execution period. For the HG source with relatively higher energies (mainly 1.17 and 1.33 MeV gamma rays from Co-60), some gamma rays penetrated the cask's shielding in the MCNP simulation and reached the surface detectors. However, as shown in Table 3, the statistical uncertainties were too large (≥50%) to be meaningful. By contrast, ADVANTG/MCNP and MAVRIC achieved substantial improvements in the computational efficiency of gamma-ray transport, especially for two cask side detectors, as indicated by their large FOMs. Compared with the ADVANTG/MCNP predictions, the 27N19G multigroup MAVRIC calculation overestimated the gamma-ray dose rates on the cask's top and side surfaces, approximately ranging from 29% to 78%. The 200N47G fine-group and continuous-energy MAVRIC calculations substantially eliminated these discrepancies and provided consistent dose rate predictions with ADVANTG/MCNP for the two gamma source problems. The perfect consistency of two continuous-energy simulations in gamma-ray transport also confirmed with great confidence that the ADVANTG/MCNP and MAVRIC calculation models built in this study were identical.

3.2. Computational efficiencies and studies

Considering the computational efficiency of Monte Carlo simulations, both ADVANTG/MCNP and MAVRIC exhibited improvements in orders of magnitude compared with the straightforward MCNP. The relative errors of their predicted dose rates on the cask surfaces were generally within 5% or smaller after a 1-day run on a single CPU core. Based on the FOM values in Table 3, ADVANTG/MCNP generally exhibited slightly higher FOMs than did MAVRIC in surface dose rate predictions. In addition, the 200N47G fine-group and continuous-energy MAVRIC calculations led to slightly deteriorated performance in computational efficiency when compared with the 27N19G coarse-group MAVRIC calculation. This small runtime penalty can be expected at the expense of higher-fidelity simulations in energy treatment.

For a hybrid deterministic/Monte Carlo simulation, the accuracy of the discrete ordinates solution affects the computational efficiency of the subsequent biased Monte Carlo simulation. In principle, the more accurate the discrete ordinates solution, the more effective is the resultant variance reduction scheme; however, this does not guarantee the best computational efficiency. The overall computational efficiency must also consider the computational overhead associated with the discrete ordinates calculations in which the mesh size of the spatial discretization is an influencing factor. The initial selection of the XYZ mesh size (98 × 98 × 58; nearly uniformly distributed) was arbitrary and based on the authors' experiences. As shown in Table 2, the two discrete ordinates calculations in forward and adjoint modes generally took less than 1 h in total, and the computational overhead was minor compared with that of approximately 1 day spent in last-step Monte Carlo simulation. Because of a variety of possible spatial discretization schemes that can be chosen, a concern regarding optimization of the FW-CADIS implementation in this problem originated from the previously selected mesh size of 98 × 98 × 58 in the XYZ coordinates, which the significant speed-ups of the ADVANTG/MCNP and MAVRIC calculations in Table 2 were based on. To address this problem, this study considered the performances of two additional spatial discretization schemes (50 × 50 × 30 and 196 × 196 × 116) by roughly halving and doubling the number of meshes in each dimension, respectively. Different discretization schemes had an effect on the execution time of the discrete ordinates tasks. The Denovo calculations with the 50 × 50 × 30 mesh discretization accelerated and could be finished in only a few minutes. By contrast, the Denovo calculations corresponding to the 196 × 196 × 116 finer mesh discretization required several hours, in particular for the FN source problem, which took almost 1 day to complete. Comparing the resultant FOMs with that of the previous mesh discretization (98 × 98 × 58) in the cask surface dose rate calculations, the results did not show any advantage and confirmed the appropriateness of the initially selected scheme that led to improved overall computational efficiency in this study.

3.3. Dose rate distributions on cask surfaces

Figs. 2 and 3 show the distributions of neutron and gamma-ray dose rates on the cask's side and top surfaces, respectively, calculated by MCNP, ADVANTG/MCNP, and three MAVRIC runs with three different cross-section sets. The general shapes of the predicted dose rate profiles were similar to each other. Focusing first on neutron dose rates around the cask, the maximal dose rate on the cask's side surface occurred near the bottom air inlets and that on the cask's top surface appeared at the air gap between the canister and the surrounding concrete cask. These phenomena were expected because of the effect of neutron streaming. The statistical uncertainties of five simulations with approximately the same computing time indicated that the computational efficiency of ADVANTG/MCNP was approximately comparable to those of the MAVRIC runs, and the FW-CADIS simulations significantly surpassed the performance of the MCNP calculation without user-specified variance reduction techniques. As shown in Fig. 2, the MCNP neutron tallies on the cask's side surface exhibited large statistical fluctuations and could not be meaningfully compared with other codes. Compared with the continuous-energy ADVANTG/MCNP calculation, the 27N19G coarse-group MAVRIC calculation underestimated the neutron dose rates on the cask's side surface by a factor of approximately two. Insufficient self-shielding correction in multigroup neutron cross sections should be the most probable cause of this discrepancy. The 200N47G fine-group MAVRIC calculation predicted higher neutron dose rates that reduced this discrepancy and approached the result of the continuous-energy MAVRIC calculation. However, the two continuous-energy calculations of ADVANTG/MCNP and MAVRIC still differed by approximately 30% in terms of the neutron dose rates on the cask's side surface.

The gamma-ray dose rates on the cask surfaces were contributed by penetrated gamma rays from the FG and HG sources and induced gamma rays from the FN source. The combined dose rate profile on the cask's side surface in Fig. 2 shows a relatively smooth distribution and has a broad peak around the middle of the effective fuel region. The streaming effect of gamma rays along air inlets

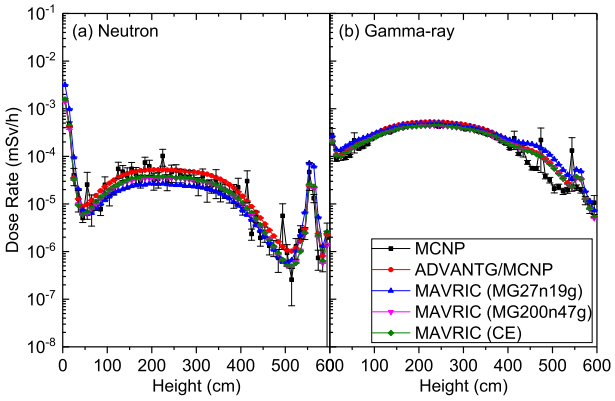

Fig. 2. Comparisons of neutron and gamma-ray dose rate distributions on the cask's side surface calculated by MCNP, ADVANTG/MCNP, and three MAVRIC runs with different cross-section sets.

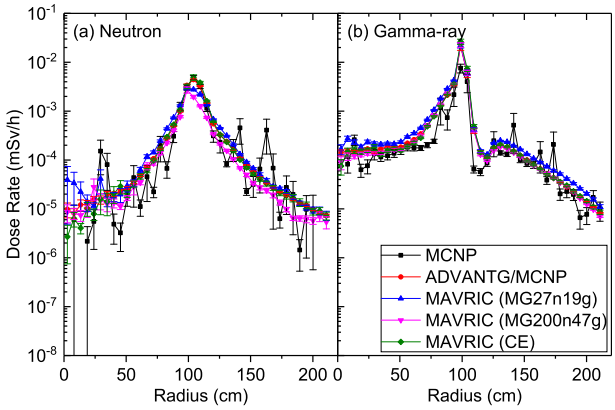

Fig. 3. Comparisons of neutron and gamma-ray dose rate distributions on the cask's top surface calculated by MCNP, ADVANTG/MCNP, and three MAVRIC runs with different cross-section sets.

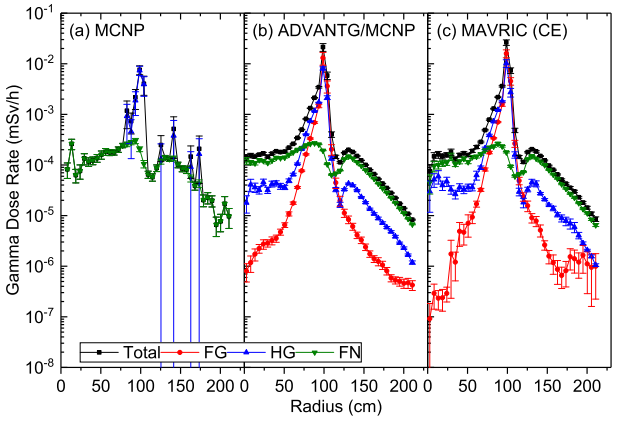

Fig. 5. Comparisons of gamma-ray dose rate distributions on the cask's top surface calculated by MCNP, ADVANTG/MCNP, and MAVRIC (CE) for three source terms (FN, FG, and HG).

was not as significant as that of neutrons. The dose rate peak on the cask's top surface still occurred at the location of the air gap surrounding the canister. Among the predictions of five Monte Carlo simulations, the resultant gamma-ray dose rates on the cask's side surface appeared more consistent with each other, except for at cask heights above 400 cm. On the cask's top surface (Fig. 3), the coarse-group MAVRIC-predicted gamma-ray dose rates were slightly higher than the ADVANTG/MCNP result. This discrepancy disappeared when the fine-group or continuous-energy MAVRIC calculations were used.

Neutron dose rates around the cask come only from the FN source term. By contrast, all three source terms (FN, FG, and HG) contributed to the gamma-ray dose rates on the cask's surfaces. Figs. 4 and 5 present the gamma-ray dose rate distributions on the cask surfaces calculated by MCNP, ADVANTG/MCNP, and MAVRIC (CE) due to the three source terms. The 1-day straightforward MCNP calculations failed to generate meaningful predictions regarding surface dose rates because of the FG and HG sources. Apparently, effective variance reduction techniques were indispensable in solving this problem. The two FW-CADIS Monte Carlo simulations demonstrated their advantages and provided generally consistent gamma-ray dose rate profiles for each of the three source terms. Among them, secondary gamma rays induced by neutron interactions were the dominant contributor of gamma-ray dose rates on the cask's surfaces, except for in two regions: (1) on the cask's side surface at heights of approximately 500 cm (Fig. 4) because of the strong and high-energy HG sources from the UEF and plenum; (2) on the cask's top surface near the air gap where the streaming and penetration of the FG and HG sources were significant and these two sources resulted in comparable contributions (as shown in Fig. 5).

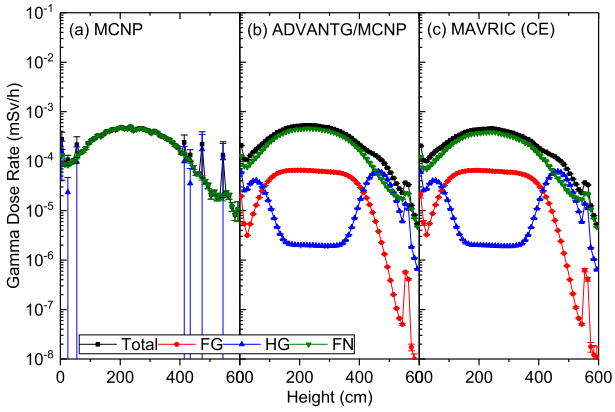

Fig. 4. Comparisons of gamma-ray dose rate distributions on the cask's side surface calculated by MCNP, ADVANTG/MCNP, and MAVRIC (CE) for three source terms (FN, FG, and HG).

3.4. Neutron and gamma-ray spectra on cask surfaces

In addition to dose rate distributions, Figs. 6 and 7 show the energy spectra of neutrons and gamma rays on the cask surfaces calculated by the two continuous-energy calculations of ADVANTG/MCNP and MAVRIC (CE). As shown in Fig. 6, the neutron spectrum on the cask's side surface consisted of two components: a small portion of source neutrons that penetrated the thick shielding of the cask and numerous thermal neutrons resulting from moderation of fast neutrons in concrete. Surprisingly, the two continuous-energy Monte Carlo calculations predicted significantly different amounts of thermal neutrons, which led to the approximately 30% difference in the neutron dose rate on the cask's side surface, as discussed in Section 3.1. The neutron spectrum on the cask's top surface was more complex than that on the cask's side surface,

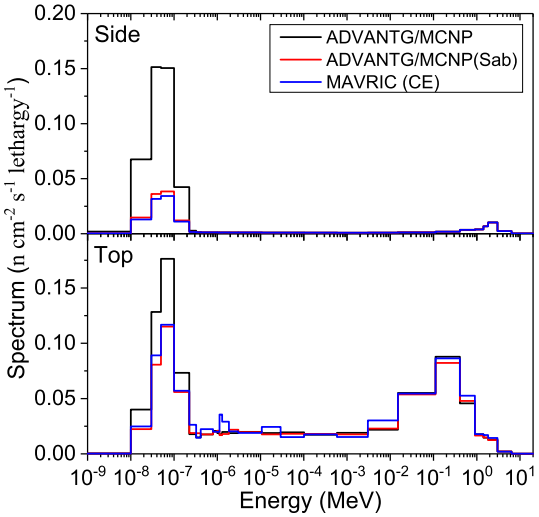

Fig. 6. Comparisons of neutron spectra on the cask's top and side surfaces calculated by ADVANTG/MCNP, ADVANTG/MCNP (Sab), and MAVRIC (CE) for the FN source term.

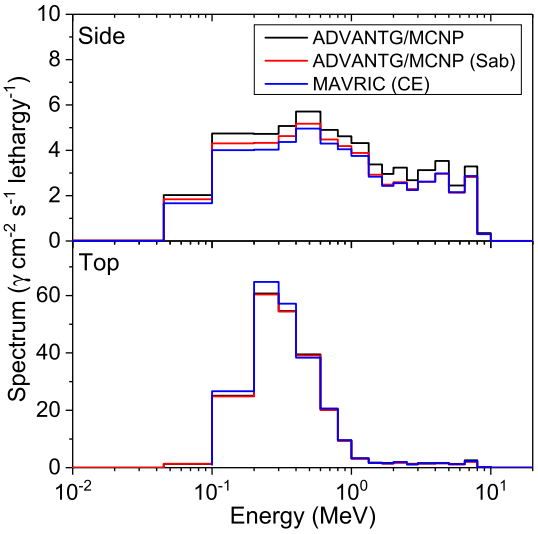

Fig. 7. Comparisons of gamma-ray spectra on the cask's top and side surfaces calculated by ADVANTG/MCNP, ADVANTG/MCNP (Sab), and MAVRIC (CE) for three source terms (FN, FG, and HG).

featuring a lot of neutrons of intermediate energies, partly because of the relatively thin shielding and partly because of the air gap between the canister and outer shield. Again, the two continuous-energy calculations of ADVANTG/MCNP and MAVRIC (CE) predicted mostly consistent energy distributions except for in the thermal neutron region. This observation led us to speculate about the inconsistency of the two calculations for neutron cross sections in this region. After a series of comparisons of neutron cross sections for each component of the concrete used in ADVANTG/MCNP and MAVRIC (CE), the authors found that the two calculations had different thermal scattering treatments for the hydrogen component in concrete. The default hydrogen ID = 1001 in the SCALE library actually referred to hydrogen in water with an S(α,β) thermal kernel [6], whereas the hydrogen ID = 1001.70c in MCNP was treated as free gas unless an additional MT card is requested by the user for a special treatment to account for thermal motion and chemical binding effects [7]. Therefore, an additional calculation denoted as ADVANTG/MCNP (Sab) with an MT card of lwtr.10t (hydrogen in light water at 293.6 K) was prepared and performed. The calculated neutron spectra on the cask's side and top surfaces are also presented in Fig. 6, and indicate overall good agreement with the MAVRIC (CE) predictions. Folding with flux-to-dose rate conversion factors, the dose rates on the cask surfaces calculated by ADVANTG/MCNP (Sab) are summarized in the last column of Table 3 for comparison. The results were in excellent agreement with MAVRIC (CE) within statistical uncertainties for all sources and detectors.

Fig. 7 shows the gamma-ray spectra on the cask's side and top surfaces calculated by three continuous-energy calculations labeled as ADVANTG/MCNP, ADVANTG/MCNP (Sab), and MAVRIC (CE), which combined the contributions from three sources (FN, FG, and HG). All calculations predicted similar energy distributions. The gamma rays on the cask's side surface had a broad energy distribution ranging from 0.05 to 10 MeV. For the cask's top surface, the gamma-ray intensity was roughly one order of magnitude higher than that on the cask's side surface, and most gamma rays were of energies within the range of 0.1–1 MeV.

Similar to Figs. 2 and 3, Figs. 8 and 9 show comparisons of neutron and gamma-ray dose rate distributions on the cask's surfaces as calculated by three continuous-energy calculations:

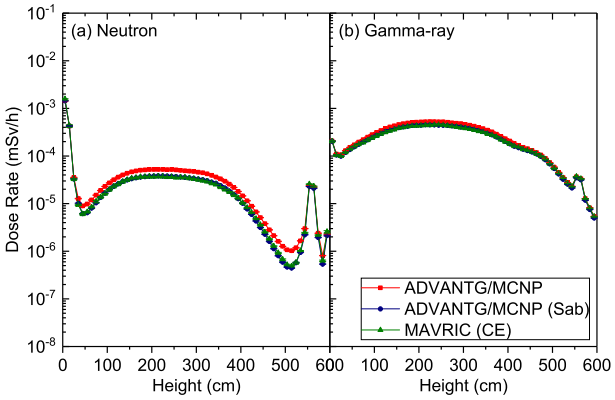

Fig. 8. Comparisons of neutron and gamma-ray dose rate distributions on the cask's side surface calculated by ADVANTG/MCNP, ADVANTG/MCNP (Sab), and MAVRIC (CE).

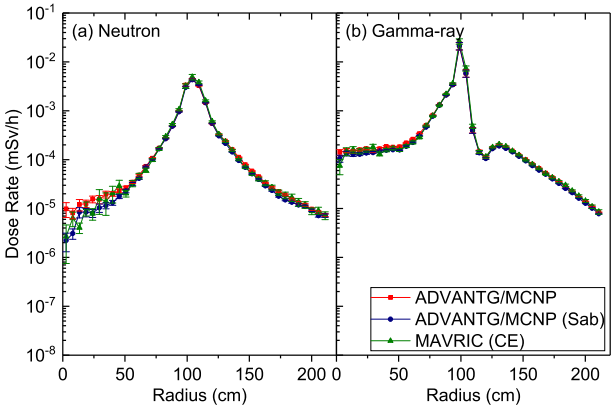

Fig. 9. Comparisons of neutron and gamma-ray dose rate distributions on the cask's top surface calculated by ADVANTG/MCNP, ADVANTG/MCNP (Sab), and MAVRIC (CE).

ADVANTG/MCNP, ADVANTG/MCNP (Sab), and MAVRIC (CE). After the inconsistent use of S(α,β) thermal scattering treatment between the two codes had been solved, ADVANTG/MCNP (Sab) and MAVRIC (CE) exhibited excellent agreement and had the same level of statistical uncertainties in this problem, indicating similar performance in terms of computational accuracy and efficiency. Although the hydrogen component represented only approximately 1% of the weight of the concrete used in this study, the calculations with and without consideration of S(α,β) thermal scattering for the hydrogen component caused approximately 30% differences in neutron dose rates on the cask's side surface, as shown in Fig. 8(a), where the neutrons had to penetrate approximately 1 m thick concrete to reach the surface and contributed to the detector. For the other surface tallies, this consideration was not so important and cannot be observed from the comparisons in Figs. 8(b) and 9.

4. Conclusions

This paper describes a real-world cask shielding problem and a systematic comparison of the two hybrid deterministic/Monte Carlo transport codes that were used to solve it. The cask shielding problem involves not only complex source and geometry configurations but also troublesome deep-penetration and streaming calculations. The Monte Carlo method is usually a preferable approach for solving such a difficult problem; however, effective variance reduction techniques are indispensable for obtaining

statistically converged results within a reasonable computing time. Aimed at obtaining the surface dose rate distributions of neutrons and gamma rays around a MAGNASTOR spent fuel storage cask, this study compared the performances of ADVANTG/MCNP and MAVRIC in terms of their prediction accuracy and computational efficiency. Both codes utilized the forward and adjoint solutions generated by the discrete ordinates Denovo code for source biasing and consistent transport biasing. However, the two hybrid codes had different FW-CADIS implementations in the last-step Monte Carlo simulation: ADVANTG was designed to directly couple with the popular continuous-energy MCNP calculation, whereas the Monte Carlo Monaco code in the latest MAVRIC sequence started to support both multigroup and continuous-energy Monte Carlo simulations.

The detailed distributions of neutron and gamma-ray dose rates on the cask's side and top surfaces were obtained from the MCNP, ADVANTG/MCNP, and MAVRIC calculations with different cross-section data sets. Compared with the straightforward MCNP calculation, the computational efficiencies of ADVANTG/MCNP and MAVRIC were substantially improved by a factor of hundreds for neutron transport; moreover, their efficiencies were markedly increased by more than several orders of magnitude for two cases involving gamma-ray sources. An examination of their FOMs revealed that the computational efficiency of ADVANTG/MCNP was slightly better than that of MAVRIC for this problem. In terms of the accuracy of predicting surface dose rates, the continuous-energy Monte Carlo simulations were considered more reliable than were the multigroup calculations, especially for problems involving the deep penetration of neutrons in complicated geometry. The comparison of ADVANTG/MCNP and three MAVRIC simulations with 27N19G, 200N47G, and CE cross-section sets supported this anticipation. When using coarse-group cross-section library 27N19G with MAVRIC, the impact of multigroup approximation led to underestimate of the neutron dose rates on the cask's side surface and overestimate the dose rates on all of the cask's surfaces for two gamma-ray sources. The 200N47G fine-group and continuous-energy MAVRIC calculations greatly improved these insufficiencies; however, the two continuous-energy calculations of ADVANTG/MCNP and MAVRIC still showed approximately 30% differences in the predicted neutron dose rates on the cask's side surface and 10%–15% differences in the induced gamma-ray dose rates on the cask's surfaces. By observing the calculated neutron spectra on the cask's surfaces, these remaining discrepancies were identified because of inconsistent use of thermal scattering treatment for hydrogen in concrete between the two codes. After this inconsistency had been solved, the ADVANTG/MCNP (Sab) and MAVRIC (CE) exhibited excellent agreement in predicting dose rates on the cask's surfaces and similar performance in terms of computational efficiency.

Acknowledgements

This work was a follow-up and expansion of our previous study presented at the International Conference on Mathematics and Computational Methods Applied to Nuclear Science and Engineering (M&C2017). It was supported by the Fuel Cycle and Material Administration of Atomic Energy Council in Taiwan, under contract no. 104FCMA018.

Appendix A. Supplementary data

Supplementary data to this article can be found online at https://doi.org/10.1016/j.net.2019.06.019.

References

[1] Taiwan Power Company, Safety Analysis Report for the ISFSI (Independent Spent Fuel Storage Installation) in Nuclear Power Plant 2, 2012.
[2] United States Nuclear Regulatory Commission, Criteria for Radioactive Materials in Effluents and Direct Radiation from an ISFSI or MRS, Report No. 10CFR72.104, 1998.
[3] J.C. Wagner, A. Haghighat, Automated variance reduction of Monte Carlo shielding calculations using the discrete ordinates adjoint function, Nucl. Sci. Eng. 128 (1998) 186–208.
[4] A. Haghighat, J.C. Wagner, Monte Carlo variance reduction with deterministic importance functions, Prog. Nucl. Energy 42 (2003) 25–53.
[5] S.W. Mosher, A.M. Bevill, S.R. Johnson, A.M. Ibrahim, C.R. Daily, T.M. Evans, J.C. Wagner, J.O. Johnson, R.E. Grove, ADVANTG - an Automated Variance Reduction Parameter Generator, ORNL/TM 2013/416 Rev. 1, 2015.
[6] Oak Ridge National Laboratory, SCALE: a Modular Code System for Performing Standardized Computer Analyses for Licensing Evaluations, Version 6.1, 2011. ORNL/TM-2005/39.
[7] X-5 Monte Carlo Team, MCNP - Version 5, Vol. I: Overview and Theory, LA-UR-03-1987, 2003.
[8] H. Thiele, F.M. Börst, Shielding benchmark calculations with SCALE/MAVRIC and comparison with measurements for the German cask CASTOR HAW 20/28 CG, Nucl. Technol. 168 (2009) 867–870.
[9] J.C. Wagner, D.E. Peplow, S.W. Mosher, T.M. Evans, Review of hybrid (deterministic/Monte Carlo) radiation transport methods, codes, and applications at Oak Ridge National Laboratory, Prog. Nucl. Sci. Technol. 2 (2011) 808–814.
[10] M. Matijević, R. Ječmenica, D. Grgić, Spent fuel pool dose rate calculations using point kernel and hybrid deterministic-stochastic shielding methods, J. Energy 65–1 (2016) 151–161.
[11] P.K. Paul, Dose rate evaluation for the ES-3100 package with HEU content using MCNP, ADVANTG, Monaco, and MAVRIC, Nucl. Technol. 205 (2019) 847–866.
[12] NAC International Inc, MAGNASTOR (Modular Advanced Generation Nuclear All-Purpose STORage) Safety Analysis Report, 2009 docket no. 72–1031.
[13] T.M. Evans, A.S. Stafford, R.N. Slaybaugh, K.T. Clarno, Denovo: a new three-dimensional parallel discrete ordinates code in SCALE, Nucl. Technol. 171 (2010) 171–200.
[14] J.C. Wagner, D.E. Peplow, S.W. Mosher, FW-CADIS method for global and semi-global variance reduction of Monte Carlo radiation transport calculations, Nucl. Sci. Eng. 176 (2014) 37–57.
[15] M.B. Emmett, J.C. Wagner, Monaco: a new 3D Monte Carlo shielding code for SCALE, Trans. Am. Nucl. Soc. 91 (2004) 701–703.
[16] B.T. Rearden, L.M. Petrie, D.E. Peplow, K.B. Bekar, D. Wiarda, C. Celik, C.M. Perfetti, A.M. Ibrahim, S.W.D. Hart, M.E. Dunn, W.J. Marshall, Monte Carlo capabilities of the SCALE code system, Ann. Nucl. Energy 82 (2015) 130–141.